0·15 dB/km. Moreover, OH absorption losses at 1·39 and 1·24 μm are also increased.

The optical loss increase in an individual cable piece was evaluated by means of an optical time domain reflectometer (OTDR) at 1·3 μm. Table 1 shows the average loss increases of cables 1–6 in repeater section A. It is found that optical losses for cables 5 and 6 increase by more than 0·4 dB/km, whereas the values are negligibly small for cables 1 and 2. The losses for cables 3 and 4 increase slightly. The difference between these cables is due to the P_2O_5 concentration in the fibres; the P_2O_5 concentrations in fibres contained in cables 5 and 6 are six and three times as much as those in fibres contained in cables 1 and 2, and 3 and 4, respectively. Therefore it is suggested that, as P_2O_5 concentration increases, the optical loss increase becomes large.

Table 1 OPTICAL LOSS CHANGE OF INDIVIDUAL CABLES IN REPEATER SECTION A

Cable	Optical loss: Just after construction	Optical loss: 2 yr after construction	Loss increase
	dB/km	dB/km	dB/km
1	0·59	0·62	0·03
2	0·60	0·59	−0·01
3	0·57	0·72	0·15
4	0·63	0·76	0·13
5	0·84	1·25	0·41
6	0·59	1·25	0·66

The splice loss stability was also examined by means of the OTDR. Fibres were spliced by the arc-fusion splice method and the spliced portion was reinforced by V-groove plastic plates.[6] Average splice loss just after construction and that in two years after construction are shown in Table 2. It is found that no loss increase occurs in splice points.

Table 2 SPLICE LOSS CHANGE OF TRANSMISSION LINES

Splice loss	Splice loss: Just after construction	Splice loss: 2 yr after construction	Loss increase
	dB	dB	dB
No. 1–2	0·11	0·07	−0·04
No. 2–3	0·10	0·12	0·02
No. 3–4	0·12	0·10	−0·02
No. 4–5	0·10	0·11	0·01

In order to clarify the origin of the loss increase, extensive studies have been made.[2,3] As a result it has been found that the phenomenon of the wavelength-dependent loss increase quite similar to that shown in Fig. 2 is observed by exposing fibres at high temperature around 200°C.[2] Moreover, it has been found that the loss increase at high temperatures is also reduced by decreasing the P_2O_5 concentration.[2] Therefore the cause of the loss increase in the actual transmission lines in the temperature range 0–40°C is also considered to be due to chemical bond changes inside the fibre among constituent atoms such as Si, Ge, P and OH.[2] The experimental result has also suggested that the behaviour of the H_2 molecule and/or H^+ ion plays a dominant role in the chemical reaction.[6] From these facts it is considered that to prevent loss increase in graded-index optical fibre transmission lines at longer wavelength regions the P_2O_5 concentration should be as small as possible. In fact, almost no loss increase is observed in the fibres with small P_2O_5 concentration as shown in Table 1.

In conclusion, wavelength-dependent optical loss increase in the graded-index optical fibre transmission lines has been observed. The loss increase becomes large in the longer-wavelength region and depends strongly on P_2O_5 concentration in the fibres. To prevent the loss increase, the P_2O_5 concentration should be as small as possible.

Acknowledgment: The authors thank N. Uchida for his valuable suggestions and discussion. The authors also thank H. Fukutomi and Y. Negishi for their encouragement and permission to submit this letter.

T. TANIFUJI
M. MATSUMOTO
M. TOKUDA

Ibaraki Electrical Communication Laboratory
Nippon Telegraph & Telephone Public Corporation
Tokai, Obaraki-ken 319-11, Japan

M. MIYAUCHI

Research & Development Bureau
Electrical Communication Laboratory
Nippon Telegraph & Telephone Public Corporation
Midori-cho, Musashino-shi, Tokyo, Japan

1st November 1983

References

1 SHIMADA, S., and UCHIDA, N.: 'Field trial of medium/small capacity optical fiber transmission system', *Rev. Electr. Commun. Lab.*, 1981, **29**, p. 1087
2 UESUGI, N., KUWABARA, T., KOYAMADA, Y., ISHIDA, Y., and UCHIDA, N.: 'Optical loss increase of phosphor-doped silica fiber at high temperature in the long wavelength region', *Appl. Phys. Lett.*, 1983, **43**, pp. 327–328
3 UESUGI, N., KUWABARA, T., OHASHI, M., ISHIDA, Y., and UCHIDA, N.: 'Stress and temperature effect on optical loss increase for phosphor-doped silica fibre in the long-wavelength region', *Electron. Lett.*, 1983, **19**, pp. 842–843
4 UCHIDA, N.: 'Design and performance of optical cables'. ICC Conference Record, 1980, p. 55.2.1
5 TANIFUJI, T., OMOTE, K., and TOKUDA, M.: 'Loss and baseband frequency response of transmission line in the field trial on medium/small capacity optical fiber transmission systems', *Rev. Electr. Commun. Lab.*, 1981, **29**, p. 1138
6 MIYAUCHI, M., MATSUMOTO, M., and HIRAI, M.: 'Practical fiber splice techniques for optical fiber cables', *ibid.*, 1981, **29**, p. 1150

'SPLIT RADIX' FFT ALGORITHM

Indexing terms: Signal processing, Fast Fourier transforms

A new $N = 2^n$ fast Fourier transform algorithm is presented, which has fewer multiplications and additions than radix 2^n, $n = 1, 2, 3$ algorithms, has the same number of multiplications as the Rader–Brenner algorithm, but much fewer additions, and is numerically better conditioned, and is performed 'in place' by a repetitive use of a 'butterfly'-type structure.

Introduction: Since the early paper by Cooley and Tukey,[1] a lot of work has been done on the FFT algorithm, and this has resulted in classes of algorithms such as radix-2^m algorithms, the Winograd algorithm (WFTA), and prime factor algorithms (PFA).

Among these, the radix-2 and radix-4 algorithms have been used most for practical applications. This is due to their simple structure, with a constant geometry (butterfly type) and the possibility of performing them 'in place', even if they are more costly in terms of number of multiplications than WFTA and PFA.

Recently, some radix-2 algorithms have been proposed[2–4] which preserve more or less the advantages mentioned above, but require less multiplications than the usual radix-2^m algorithms. Unfortunately, these methods need 20–30% more additions, and seem to be numerically ill conditioned.

We present here an algorithm which includes the advantages of these radix-2^m methods:

(*a*) the lowest number of multiplications, together with real-factor algorithms

(*b*) the lowest number of additions among the 2^m algorithms

(*c*) the same regularity as radix-4 algorithms when implemented through an autogen method[9]

(*d*) as flexible as radix-2 algorithms (useful for all $N = 2^n$)

(*e*) numerically as well conditioned as the radix-4 algorithm.

'Split-radix' algorithm: This algorithm comes from a very simple observation: a radix-2 algorithm diagram can be transformed quite straightforwardly into a radix-4 algorithm diagram only by changing the exponents of the twiddle factors. When doing so, it is quite clear that, at each stage of the algorithm, a radix-4 is best for the odd terms of the DFT, and radix-2 for the even terms of the DFT. So one might guess that restricting the transformation above locally to the lower part of the diagram only might improve the algorithm. It turns out that this is indeed the case.

The 'split-radix' algorithm is then based on the following decomposition: if

$$X_k = \sum_{n=0}^{N-1} x_n W^{nk}$$

is to be computed, it is decomposed as

$$\begin{aligned} X_{2k} &= \sum_{n=0}^{N/2-1} (x_n + x_{n+(N/2)}) W^{2nk} \\ X_{4k+1} &= \sum_{n=0}^{N/4-1} [(x_n - x_{n+(N/2)}) \\ &\quad + j(x_{n+(N/4)} - x_{n+3(N/4)})]\, W^n W^{4nk} \\ X_{4k+3} &= \sum_{n=0}^{N/4-1} [(x_n - x_{n+(N/2)}) \\ &\quad - j(x_{n+(N/4)} - x_{n+(3N/4)})] W^{3n} W^{4nk} \end{aligned} \qquad (1)$$

The first stage of a split-radix decimation in frequency decomposition then replaces a DFT of length N by one DFT of length $N/2$ and two DFTs of length $N/4$ at the cost of $[(N/2) - 4]$ general complex multiplications (3 real multiplications + 3 additions), and 2 multiplications by the eighth root of unity (2 real multiplications + 2 additions).

The length-N DFT is then obtained by successive use of such decompositions up to the last stage, where some usual radix-2 butterflies (without twiddle factors) are needed (see Fig. 1 for a length-32 split-radix FFT).

Complexity: By iterating the decomposition given in eqn. 1, we can easily obtain the number of multiplications (Table 1) and additions (Table 2) required to compute a length-N DFT by using the split-radix algorithm.

Observations of Tables 1 and 2 show that the split-radix algorithm has the lowest number of multiplications, together with the Rader–Brenner algorithm, and the lowest number of additions.

Table 1 NUMBER OF NONTRIVIAL REAL MULTIPLICATIONS TO COMPUTE A LENGTH-N COMPLEX DFT

N	Radix-2	Radix-4	Radix-8	Rader–Brenner[2]	Preuss[4]	Split-radix
16	24	20		20	20	20
32	88			68	68	68
64	264	208	204	196	196	196
128	712			516	516	516
256	1800	1392		1284	1284	1284
512	4360		3204	3076	3076	3076
1024	10248	7856		7172	7172	7172

It is interesting to notice that this same number of multiplications for the Rader–Brenner and split-radix algorithms are obtained by completely different approaches. The split-radix algorithm is also numerically better conditioned than the Rader–Brenner algorithm (it uses partly the same factors as the radix-4 algorithm).

It is also interesting to notice that the number of twiddle factors (j, $\sqrt[8]{1}$, W^k) is exactly the same in radix 2–4–8 and

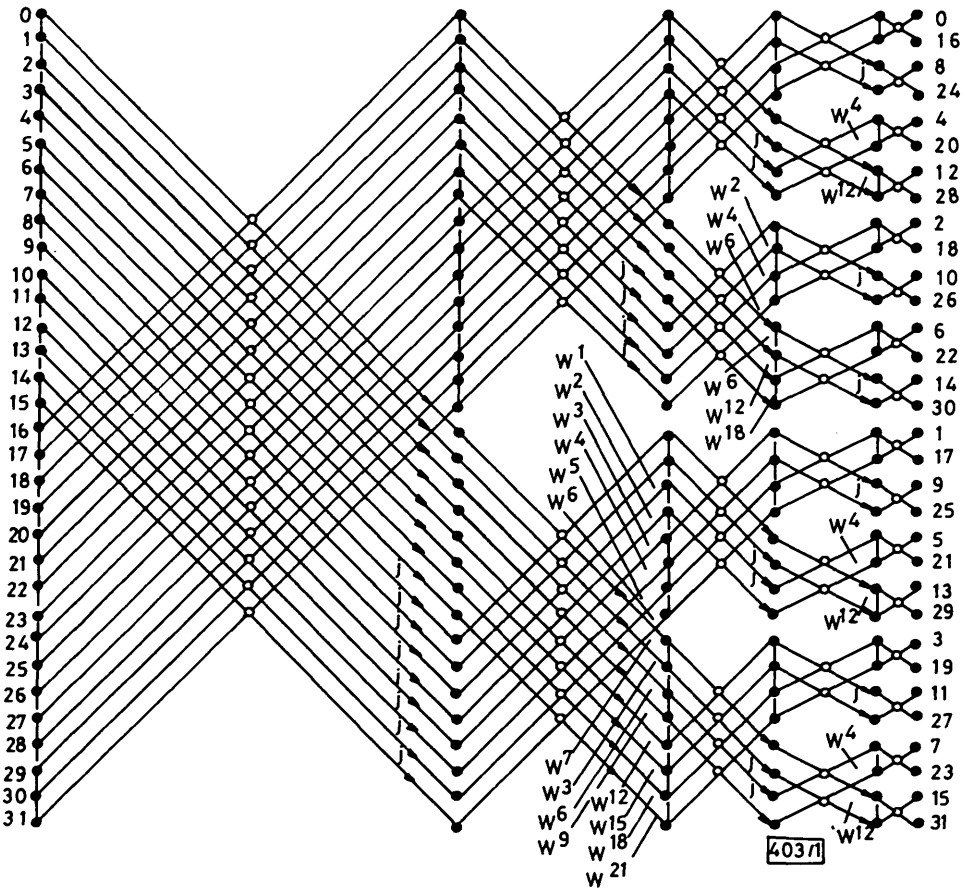

Fig. 1 *32-point, in-place, split-radix FFT*

Table 2 NUMBER OF REAL ADDITIONS TO COMPUTE A LENGTH-N COMPLEX DFT

N	Radix-2	Radix-4	Radix-8	Rader–Brenner[2]	Preuss[4]	Split-radix
16	152	148		148	172	148
32	408			424	448	388
64	1032	976	972	1104	1124	964
128	2504			2720	2728	2308
256	5896	5488		6464	6444	5380
512	13566		12420	14976	14896	12292
1024	30728	28336		34048	33844	27652

split-radix algorithm, and even variable radix, as proposed in Reference 6, but that the split-radix has the lowest number of nontrivial multiplications.

Another remark is that the split-radix algorithm closely follows the demonstration in Reference 7 of the computational complexity of a 2^n DFT (although it has not been proved optimum).

We can also notice that computing the odd terms of the split-radix DFT through a higher radix (8, for example) does not improve the algorithm.

Implementation: The split-radix algorithm can be performed in place by repetitive use of the 'butterfly' type of structure given in Fig. 2.

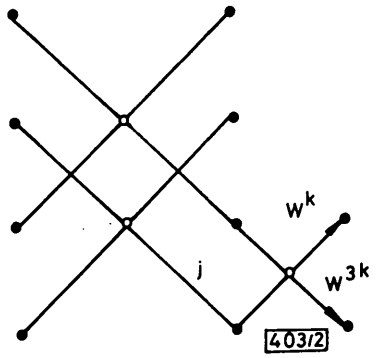

Fig. 2 *The 'butterfly' used in the split-radix algorithm*

Notation:

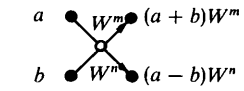

The implementation of the algorithm is considerably simplified by noting that at each stage i of the algorithm the butterflies are always applied in a repetitive manner to blocks of length $N/2^i$. Then only one test is needed to decide whether the butterflies are applied to the block or not (2^i tests at each stage i).

In fact, when using the 'autogen' technique[9] the implementation is still easier (no test at all—they are precomputed). Also notice that the minimum number of multiplications is obtained by using only four types of butterflies.

Conclusion: The split-radix has been proposed for FFT computations, and we believe it is a good candidate for fast Fourier transformation on digital signal processors, since it has the lowest number of arithmetic operations for length $N = 2^n$. The programs are available on request, and more details on the implementation will be given in a forthcoming paper.

P. DUHAMEL
H. HOLLMANN
CNET/PAB/RPE
38–40 rue du Général Leclerc
92131 Issy-les-Moulineaux, France

8th November 1983

References

1 COOLEY, J. W., and TUKEY, J. W.: 'An algorithm for machine computation of complex Fourier series', *Math. Comput.*, 1965, **19**, pp. 297–301
2 RADER, C. M., and BRENNER, N. M.: 'A new principle for fast Fourier transformation', *IEEE Trans.*, 1976, **ASSP-24**, pp. 264–265
3 CHO, K. M., and TEMES, G. C.: 'Real-factor FFT algorithms'. Proceedings 1978 IEEE ICASSP, pp. 634–637
4 PREUSS, R. D.: 'Very fast computation of the radix-2, discrete Fourier transform', *IEEE Trans.*, 1982, **ASSP-30**, pp. 595–607
5 NUSSBAUMER, H. J.: 'Fast Fourier transform and convolution algorithm' (Springer Verlag, 1981)
6 JOHNSON, H., and BURRUS, C. S.: 'Twiddle factors in the radix-2 FFT'. Proceedings 1982 Asilomar Conference on circuits, systems and computers, pp. 413–416
7 WINOGRAD, S.: 'On the multiplicative complexity of the discrete Fourier transform' *in* 'Advances in mathematics Vol. 32', 1979, pp. 83–117
8 BURRUS, C. S., and ESCHENBACHER, P. W.: 'An in-place, in-order prime factor FFT algorithm', *IEEE Trans.*, 1981, **ASSP-29**, pp. 806–817
9 MORRIS, L. R.: 'Automatic generation of time efficient digital signal processing software', *ibid.*, 1977, **ASSP-25**, pp. 74–79

LONG-WAVELENGTH TRANSIMPEDANCE OPTICAL RECEIVER PERFORMANCE ENHANCEMENT USING COOLED GERMANIUM AVALANCHE PHOTODIODES

Indexing terms: Optoelectronics, Avalanche photodiodes

An optical sensitivity improvement of 1·5 dB was produced by moderate cooling of a commercially available 100 μm p^+-n Ge APD in a transimpedance receiver, built on a standard printed circuit board. At 1·3 μm and 140 Mbaud, −45·2 dBm was achieved, making this receiver highly competitive where cooling is permitted.

Introduction: Ge APDs have been regarded as unsatisfactory for use in the 1·3 to 1·5 μm wavelength range due to their large and temperature-dependent leakage current. With the present commercially available p^+-n devices, however, good performance may be obtained at temperatures of 25°C and below. For some applications, the use of simple Peltier-effect cooling is permissible, thus reducing excess noise generated by avalanche multiplication of thermally generated electron-hole pairs[1] which, otherwise, is the dominant source of impairment up to 140 Mbaud.[2] This letter describes recent work with commercially available, shallow-junction p^+-n 100 μm-diameter Ge APDs showing how thermoelectric cooling can give significant improvements in receiver performance.

Experimental APD assessment: The total dark current variation with temperature for a commercial p^+-n 100 μm Ge APD (NDL 5100P) was empirically assessed using a standard environmental chamber flushed with dry nitrogen gas to eliminate condensation effects. Diffusion effects dominated above 273 K as expected. Separation of the unmultiplied bulk and surface leakage currents was carried out using a standard technique.[3] At 293 K, the surface and unmultiplied bulk leakage currents were estimated to be 120 and 20 nA, respectively. Quantum efficiency, Miller index and ionisation ratio figures were available from tests similar to previous work at BTRL.[1]

Theoretical analysis: APD transimpedance receiver sensitivity was calculated using the theory of Smith and Garrett.[4] This is based on a Gaussian approximation which is adequate under many practical conditions. The mean optical power P_{av} for a given bit error ratio (BER) is determined by

$$P_{av} = \frac{Qhc}{2T\lambda\eta}\left[QF_p I_2 + \left(\frac{2}{M_p}\right)\left[Z + \frac{T}{q} I_2 I_b M_d^2 F_d\right]^{1/2}\right] \quad (1)$$

where $Q = 6$ for 10^{-9} BER, T is the bit spacing (7·1 ns) and I_2 is the normalised Personick integral for NRZ pulses (1·127). The optical constants in eqn. 1, h, c, λ and η, are Planck's constant, velocity of light, optical wavelength (1·3 μm) and quantum efficiency (67%), respectively. APD parameters M_p, M_d, F_p, F_d and I_b are based on the McIntyre model and are